# Rainfall and Radiative Heating Rates from TOGA COARE Atmospheric Budgets

RICHARD H. JOHNSON AND PAUL E. CIESIELSKI

*Department of Atmospheric Science, Colorado State University, Fort Collins, Colorado*

(Manuscript received 18 December 1998, in final form 6 July 1999)

ABSTRACT

Atmospheric heat and moisture budgets are used to determine rainfall and radiative heating rates over the western Pacific warm pool during the Tropical Ocean Global Atmosphere Coupled Ocean–Atmosphere Response Experiment (TOGA COARE). Results are compared to independent estimates of these quantities from the other sources. Using the COARE bulk flux algorithm to estimate surface evaporation over the intensive flux array (IFA), the IFA moisture budget-derived average rainfall for the 120-day intensive observing period (IOP) is 8.2 mm day$^{-1}$. This value agrees closely with recent estimates from satellites and the ocean salinity budget. For a smaller area within the IFA containing the rain-mapping domain of the TOGA and Massachusetts Institute of Technology 5-cm radars, the atmospheric budget for the 101-day radar deployment yields 6.8 mm day$^{-1}$, slightly greater than the independent radar rain rate estimate of 5.4 mm day$^{-1}$.

Comparison of budget-derived rainfall with National Centers for Environmental Prediction and European Centre for Medium-Range Weather Forecasts reanalyses indicates that the reanalyses produce excessive precipitation in the northern ITCZ (around 10°N) in association with anomalously moist low-level conditions at those latitudes. These anomalous conditions arise from moist-biased VIZ humidity sensors on rawinsondes launched at operational sites there, while outside those latitudes dry-biased Vaisala sensors were almost exclusively used.

Computation of the vertically integrated net radiative heating rate $\langle Q_R \rangle$ as a residual from the heat and moisture budgets reveals a ~1.5 K day$^{-1}$ variation on the timescale of the Madden–Julian oscillation. The implied horizontal variation of $\langle Q_R \rangle$ is large enough to have significant impacts on the tropical Walker and Hadley circulations. The IFA–IOP mean $\langle Q_R \rangle$ is −0.41 K day$^{-1}$. This net cooling rate is less than many previous estimates for the Tropics but is within the range of independent estimates for COARE based on radiation models and observations. This small value may arise from decreased longwave emission to space due to abundant cirrus over the warm pool and, in addition, may reflect some shortwave absorption by cirrus, but not necessarily ''anomalous absorption'' as has been recently proposed.

## 1. Introduction

A primary objective of the Tropical Ocean Global Atmosphere Coupled Ocean–Atmosphere Response Experiment (TOGA COARE) is the determination of the principal processes responsible for the coupling of the ocean and atmosphere in the western Pacific warm pool region (Webster and Lukas 1992). Precipitation associated with deep convection represents a central aspect of this coupling. Recognizing that there is no ''best'' method for measuring rainfall over tropical oceans, COARE was designed to employ a variety of techniques—rain gauges, remote sensing (atmospheric profilers, satellites, radars), atmospheric budgets, upper-ocean budgets, and numerical prediction models—from which the results could be analyzed and synthesized to yield an integrated view of warm pool precipitation.

Results from three ~1-month shipboard deployments of the Massachusetts Institute of Technology (MIT) and TOGA radars within the COARE intensive flux array (IFA) indicate an intensive observing period (IOP)–average rainfall rate (corrected for range dependence) of 5.4 mm day$^{-1}$ for the ~400 km east–west, by 300 km north–south rain-mapping domain covering about half the IFA area (Short et al. 1997; Godfrey et al. 1998). Short et al. point out that this estimate is generally much smaller (by a factor of 2–3) than shipboard and buoy-mounted optical rain gauge (ORG) measurements, whose records may be subject to spurious peaks due to vibration. It is also somewhat smaller (by 30%) than the average of IOP estimates derived from over 50 geostationary and polar-orbiting satellite rainfall algorithms for the larger area of the IFA (Ebert and Manton 1998). Rainfall rates for COARE have also been diagnosed from atmospheric budgets: from the heat and moisture budgets by Frank et al. (1996) and from the moisture budget by Lin and Johnson (1996b). IOP-mean values for the IFA reported by those studies differ considerably: 9.1 mm day$^{-1}$ from the heat budget by Frank et al. (1996), after applying the correction suggested in their

*Corresponding author address:* Dr. Richard H. Johnson, Department of Atmospheric Science, Colorado State University, Fort Collins, CO 80523.
E-mail: rhj@vortex.atmos.colostate.edu

appendix, and 5.6 mm day$^{-1}$ from the moisture budget by Lin and Johnson (1996b). These differences will be addressed in this paper. But more importantly, results to date from COARE atmospheric budgets have not been directly compared to radar-determined rainfall rates for the areas and times represented by the radar measurements, nor have they been compared to other independent estimates. One of the purposes of this study is to conduct such comparisons. In doing so, we will take into account recent improvements to the sounding wind profiles by merging data from the 915-MHz wind profilers in the IFA (Ciesielski et al. 1997). The other comparisons that will be considered include the Climate Prediction Center (CPC) Merged Analysis of Precipitation (CMAP; Xie and Arkin 1997), the mixed microwave–visible–infrared satellite rain estimation algorithm of Curry et al. (1999), and the ocean salinity budget analysis of Feng et al. (1998).

In addition, the budget-derived rainfall will be compared to results from the National Centers for Environmental Prediction (NCEP) reanalysis (Kalnay et al. 1996) and the European Centre for Medium-Range Weather Forecasts (ECMWF) reanalysis (Gibson et al. 1997). An evaluation will be given of the reliability of the NCEP and ECMWF reanalysis meridional rainfall distributions over the COARE domain.

Last, the vertically integrated heat and moisture budgets will be combined to determine the tropospheric-averaged net radiative heating rate $\langle Q_R \rangle$. This computation requires estimates of the surface sensible and latent heat fluxes, which have been determined with great accuracy in COARE (Fairall et al. 1996; Weller and Anderson 1996). The mean values of $\langle Q_R \rangle$ for the IOP will be compared to independent estimates prepared by other investigators based on surface and top-of-the-atmosphere measurements and radiation models with assumed moisture and cloud distributions. An important question is whether the tropospheric radiative characteristics over the warm pool are different from other tropical regions that have been studied. For example, Harshvardhan et al. (1989), Stephens et al. (1994), and Bergman and Hendon (1998) show that longwave and shortwave cloud radiative forcings over the warm pool and eastern Indian Ocean are greater than other locations around the globe. This horizontal variability can have substantial impacts on the tropical Walker and Hadley circulations (Hartmann et al. 1984; Slingo and Slingo 1988, 1991; Randall et al. 1989; Sherwood et al. 1994; Webster 1994; Raymond 2000). Also, these results and comparisons will have a direct bearing on the recent claims by Cess et al. (1995), Ramanathan et al. (1995), and Pilewskie and Valero (1995) of anomalous absorption by tropical cirrus.

## 2. Analysis procedures

### *a. Methods*

Following Yanai et al. (1973) and Yanai and Johnson (1993), the integration of the conservation laws for heat and moisture from the tropopause pressure $p_T$ to surface pressure $p_s$ yields

$$\langle Q_1 \rangle = \langle Q_R \rangle + LP + S \tag{1}$$

$$\langle Q_2 \rangle = L(P - E), \tag{2}$$

where $Q_1 \equiv c_p[(\partial\overline{T}/\partial t + \overline{\mathbf{v}} \cdot \nabla\overline{T} + (p/p_0)^{\kappa}\overline{\omega}\partial\overline{\theta}/\partial p)]$ is the apparent heat source; $Q_2 \equiv -L(\partial\overline{q}/\partial t + \overline{\mathbf{v}} \cdot \nabla\overline{q} + \overline{\omega}\partial\overline{q}/\partial p)$ the apparent moisture sink; $q$ the specific humidity; $\theta$ the potential temperature; $\kappa = R/c_p$; $R$ and $c_p$ gas constant and specific heat at constant pressure for moist air, respectively; $L$ the temperature-dependent latent heat of vaporization; $P$ precipitation rate; $S$ sensible heat flux; $E$ evaporation rate; overbar denotes a horizontal average; and $\langle\ \rangle \equiv (1/g)\int_{p_T}^{p_s}(\ )\,dp$. Hydrometeor storage effects are neglected in (1) and (2) since the primary application here is to long time averages ($\sim$weeks and longer). However, on short timescales (e.g., daily averaged rainfall estimates, to be presented later) cloud storage terms can be important (McNab and Betts 1978). Nevertheless, because of the difficulty in determining changing cloud fields as a function of height (Johnson 1980), storage effects have been excluded in this study. In addition, frictional heating arising from dissipation of kinetic energy is neglected in (1) (Betts 1974).

The approach here is to use the moisture budget (2) to determine the precipitation rate $P$ as a residual. Using the technique outlined below, $Q_2$ is determined from sounding data, and $E$ is computed by applying the bulk flux algorithm of Fairall et al. (1996) to mooring data within the IFA using a procedure described in Lin and Johnson (1996b). An alternative method for obtaining $P$ involves the use of the heat budget (1). However, this approach requires a determination of tropospheric-mean net radiative heating rate $\langle Q_R \rangle$, a quantity that has considerable uncertainty over the warm pool. Therefore, we will restrict computations of $P$ to (2) but will employ the combined form of (1) and (2) to determine $\langle Q_R \rangle$ as a residual from

$$\langle Q_1 \rangle - \langle Q_2 \rangle = \langle Q_R \rangle + S + LE. \tag{3}$$

The results will be compared to independent computations of $\langle Q_R \rangle$ by other investigators.

Two previous studies have reported precipitation rates from COARE atmospheric budgets. Frank et al. (1996) used a line-integral technique to determine mass divergence over the IFA and surrounding sounding polygons, and Lin and Johnson (1996b) used the iterative weighted average interpolation scheme of Barnes (1964, 1973). In our study we have experimented with three different techniques: the Barnes scheme, Ooyama's (1987) cubic spline interpolation scheme, and the multiquadric interpolation scheme of Nuss and Titley (1994). Owing to the difficulty in prescribing boundary conditions in data-sparse areas near the edge of the analysis domain, problems were encountered with the cubic spline scheme, which narrowed the choices to the Barnes and

multiquadric schemes. Several tests (to be discussed later) indicate the multiquadric scheme performs best. This scheme, referred to as MQD, is based on the general theory of interpolation using circular hyperboloid radial basis functions. Values of three free parameters used in the application of the MQD scheme (Nuss and Titley 1994) are described in the appendix.

The vertical motion $\omega$ in $Q_1$ and $Q_2$ is computed by integrating the mass continuity equation from the surface to 75 hPa. The vertical velocity was set to zero at that level by applying a constant adjustment to the vertical divergence profile. However, since the average tropopause height over the IFA was ~90 hPa, $Q_1$ was set to zero for $p \leq 100$ hPa.

The computation of $\langle Q_R \rangle$ from (3) is sensitive to small errors since it depends on the difference between two large quantities $\langle Q_1 \rangle$ and $\langle Q_2 \rangle$. Therefore, several additional considerations are made to refine its estimate, all of which act in the direction of increasing the diagnosed cooling rate.

- Effect of rain on computation of $\omega$.

  The net removal of mass by rain (precipitation $P$ removing mass, ocean-surface evaporation $E$ adding it) affects divergence and computed $\omega$. This effect is normally neglected in budget studies, but may be important when it is raining heavily or for long-term integrations (Trenberth 1991; Trenberth et al. 1995). A revised form of mass continuity to include this effect is

$$\frac{1}{M}\frac{dM}{dt} + \nabla \cdot \mathbf{v} + \frac{\partial \omega}{\partial p} = 0, \tag{4}$$

  where the first term in (4) is the fractional rate of change of mass at each level due to net condensation.

  Ordinarily, it is assumed that $dM/dt = 0$, which yields the standard mass continuity equation in isobaric coordinates. However, if there is a removal of mass from the column by net condensation then the first term on the lhs is not zero (Trenberth 1991). The mass sink due to net condensation $P$ is distributed vertically whereas the mass source due to evaporation $E$ is at the ocean surface.

  Assuming the bulk of the condensate production takes place over a lower-tropospheric depth $\Delta z$, then the fractional change in mass over this depth due to net condensation is

$$\frac{1}{M}\frac{dM}{dt} = \frac{1}{\rho \Delta z}(P - E)\rho_w, \tag{5}$$

  where $\rho$ is the total density of air (consisting of dry air, vapor, and condensate) and $\rho_w$ is the density of water. This equation represents a correction to the divergence. Assuming $\Delta z = 5$ km, (5) can be written as

$$\frac{1}{M}\frac{dM}{dt} = 2.9 \times 10^{-9}\,(P - E)\ \text{s}^{-1}$$

$$[P - E \text{ in mm day}^{-1}]$$

  For the IOP–IFA-mean $P - E$ of ~5 mm day$^{-1}$, the divergence correction is rather small, $1.5 \times 10^{-8}$ s$^{-1}$, which reduces the lhs of (3) by 0.01 K day$^{-1}$. However, at times of heavy rainfall, say an extreme area-averaged value of 10 mm h$^{-1}$, the correction can be large, $0.7 \times 10^{-6}$ s$^{-1}$.
- Sensible heat flux due to rain.

  Gosnell et al. (1995) estimate the sensible heat flux due to rain (which falls near the wet-bulb temperature, about 3 K colder than the air) at about 2 W m$^{-2}$ over the warm pool, with values up to several hundred watts per meter squared during the heaviest rain episodes. This effect, a cooling of the ocean but heating of the atmosphere, is represented by an additional term on the rhs of (3) of ~0.02 K day$^{-1}$ for the IOP.
- Frictional dissipation associated with rainfall.

  Emanuel and Bister (1996) show that there is an increase in internal energy due to frictional dissipation associated with falling precipitation given by $\rho g l V_T$, where $l$ is the precipitation mixing ratio and $V_T$ is the terminal velocity. Integrated with altitude, this is just the surface precipitation rate times $g$ times the average altitude the precipitation traverses on its way down. For an 8 mm day$^{-1}$ IOP-mean rainrate and a fall distance of 3 km, this effect represents an additional 0.02 K day$^{-1}$ on the rhs of (3).

While the impacts of these processes (including humidity biases discussed in section 2c) on budget results are generally rather small and, hence, normally neglected, they are considered here in the computation of $\langle Q_R \rangle$. Since three of them are directly proportional to rainfall rate, their cumulative effect on the diagnosed $\langle Q_R \rangle$ during heavy rainfall periods (e.g., mid-December) may be significant. They may also explain some of the ''climate drift'' (enthalpy loss) in long-term integrations of cloud-resolving or single-column models that use the advective terms from the atmospheric budgets as large-scale forcing (e.g., Emanuel and Živković-Rothman 1999).

### b. Data

The Intensive Flux Array (IFA) is a polygon defined by the four sounding sites Kapingamarangi, R/V *Kexue 1*, R/V *Shiyan 3*, and Kavieng (Fig. 1). Since we use an objective analysis technique, sounding data from both inside and outside the IFA influence computed fields of divergence and vertical motion for the IFA region. The outer polygon in Fig. 1 is the outer sounding array (OSA). Six-hourly sounding data were objectively analyzed onto a 1° by 1° grid at 25-hPa intervals from 1000 to 25 hPa over an area extending well beyond that shown in Fig. 1 (from 20°S–20°N to 130°E–170°W) that includes surrounding operational sounding stations.

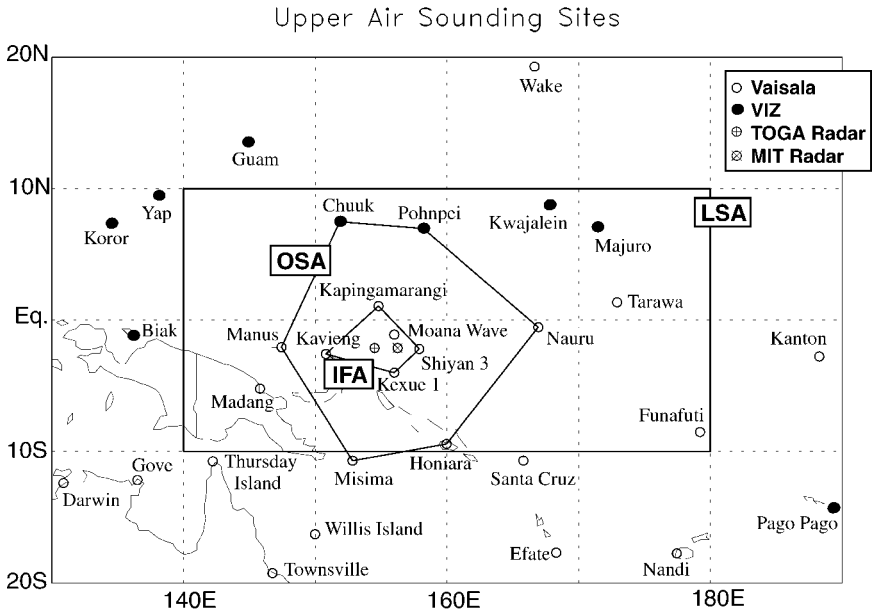


FIG. 1. Upper-air sounding sites in the TOGA COARE region. Large-Scale Array (LSA), Outer Sounding Array (OSA), and Intensive Flux Array (IFA) are indicated. Vaisala sites, open circles; VIZ sites, closed circles.

Quality control procedures and other details of the sounding dataset can be found in Lin and Johnson (1996a). In addition to those procedures, the raw sounding data from sites with integrated sounding systems (ISSs; Parsons et al. 1994) have been augmented by 915-MHz wind profiler data to fill in for gaps in the ISS Omegasonde winds that arose due to signal problems. The procedure to merge the Omegasonde and profiler winds is described in Ciesielski et al. (1997). The merging procedure has only a minor effect on the IOP-mean rainfall; however, for shorter periods, for example, the late-December westerly wind burst, the effect on computed rainfall rates is significant.

The reliability of the rainfall and radiative heating rate estimates depends critically on the accuracy of the surface fluxes. Fortunately, considerable effort was expended in COARE to obtain accurate surface sensible and latent heat fluxes within the IFA. Particularly important was the placement of the improved Meteorological surface mooring (IMET) near the center of the IFA (Weller and Anderson 1996). Surface sensible and latent heat fluxes computed with IMET data using the COARE bulk aerodynamic algorithm (Fairall et al. 1996) agreed with directly measured, three-cruise averaged fluxes from R/Vs *Moana Wave* and *Wecoma* to better than 2.5 and 4.0 W $m^{-2}$, respectively (Weller and Anderson 1996). Since IFA-averaged fluxes are required for the budget computations, and only point measurements are available, we approximate the IFA-mean surface latent heat flux by averaging the IMET values with those determined by the COARE bulk flux algorithm applied to data from three TOGA Thermal Array in the Ocean Automated Temperature Line Acquisition System (McPhaden 1993) buoys in the IFA. Lin and Johnson (1996b) show that IOP time series of the fluxes from the individual buoys agree rather well, suggesting that fluxes are coherent over a relatively large area, at least on long (~day) timescales. Surface fluxes for the OSA and large-scale array (LSA; 10°S–10°N and 140°E–180°) were determined by a procedure described in Lin and Johnson (1996b) whereby ECMWF surface fluxes were adjusted over these respective areas by the ratio of the IMET flux to the ECMWF flux at the IMET position at each 6-h sounding time.

The NCEP and ECMWF reanalysis fields used in this study are based upon their T62 (~210-km horizontal resolution) and T106 (125-km resolution) models, respectively. To determine IFA-averaged rainfall rates from the reanalyses, values from the native resolution were interpolated onto a 1° latitude × longitude grid to match the MQD resolution, and IFA means were computed by taking the average of the grid points falling within the IFA.

The radar data are taken from Short et al. (1997) based on observations from the MIT and TOGA 5-cm radars aboard the R/Vs *Vickers* and *Xiangyanghong 5*, respectively. Short et al. determined rainfall rate $R$ from radar reflectivity $Z$ data using separate $Z$–$R$ relationships for convective and stratiform precipitation.

Satellite rainfall estimates for the IFA are obtained from two techniques: 1) the mixed rainfall algorithm of Curry et al. (1999), and (2) the CMAP of Xie and Arkin (1997). The Curry et al. scheme, based on the work of Sheu et al. (1996), combines visible and infrared (IR) sampling from geostationary satellites with microwave rainfall retrievals from polar-orbiting satellites. The

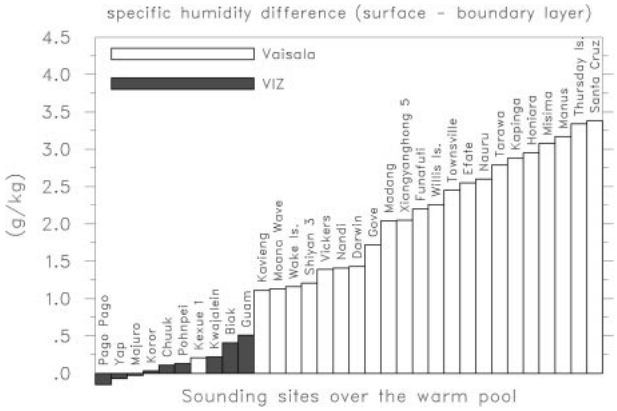


FIG. 2. Difference between the surface and boundary layer mean specific humidity $\Delta q$ for the sounding sites shown in Fig. 1, where boundary layer mean $q$ is defined as the average $q$ from the first sounding point above the surface to 960 hPa. Vaisala sites, clear; VIZ sites, shaded.

CMAP analysis consists of a merger of rain gauge data with a variety of IR and microwave satellite estimates. Because CMAP has only monthly or pentad values for the COARE period, rainfall estimates are also made using the IR-based Geostationary Operational Environmental Satellite (GOES) precipitation index (GPI; Arkin and Meisner 1987). While the GPI is known to overestimate rainfall (Ebert and Manton 1998), it is used here principally to infer temporal variability of rainfall over the COARE region. The GPI was computed using digitized Japanese *GMS-4* satellite brightness temperature data at 10-km horizontal resolution provided by Dr. Tetsuo Nakazawa.

### c. Impact of sounding humidity errors

Shortly after the field phase of COARE it became apparent that the humidity sensors on the various sounding systems in the COARE domain exhibited a variety of errors (Zipser and Johnson 1998; Lucas and Zipser 2000). The Vaisala H-Humicap sensors used at the ISS sites (see Fig. 1 for geographical distribution of humidity sensor types) were generally too dry (by ~5%) in the boundary layer owing to a contamination of the dielectric polymer by aging packaging material. The Vaisala A-type sensor used at other COARE priority sites also exhibited a dry bias, though its characteristics have yet to be determined. In contrast, the VIZ hygristor used on soundings around 10°N displayed a moist bias (Wade and Schwartz 1993). This contrasting behavior of the VIZ and Vaisala humidity sensors is shown in Fig. 2, a histogram of the difference $\Delta q$ between the surface specific humidity $q$ (measured by the surface weather station at the sounding site) and the near-surface to 960-hPa average $q$ (measured by the sonde). As discussed by Zipser and Johnson (1998), evidence from low-level COARE aircraft measurements combined with surface measurement and Monin–Obukhov similarity theory indicates that $\Delta q$ should be ~1 g kg$^{-1}$. However, Fig. 2 shows that for many of the Vaisala sites, $\Delta q$ far exceeds 1 (indicating a sensor dry bias, assuming the surface measurement of $q$ is accurate), whereas $\Delta q$ for most of the VIZ sites is much less than 1 (indicating a sensor moist bias).

Sensitivity tests show that the impacts of these errors on the results of this study, diagnosed rainfall and radiative heating rates, are relatively small, <3% and 10%, respectively. Nevertheless, as will be discussed later, their impact on cloud-scale and numerical models may be large because potential energy available for convection and convective triggering are very sensitive to boundary layer moisture.

## 3. Mean profiles of $Q_1$ and $Q_2$

Contoured frequency by altitude diagrams (CFADs; Yuter and Houze 1995) of IFA-mean $Q_1$ and $Q_2$ computed for the IOP are shown in Fig. 3. The frequencies of $Q_1$ and $Q_2$ are skewed toward positive values, representing heating and drying; however, the CFADs show that they are a residual of numerous large positive *and* negative values. The large positive values in the middle to upper troposphere are indicative of frequent deep convection, whereas many of the negative values in the low to middle troposphere are associated with evaporation and melting in the ''stratiform'' components of mesoscale convective systems (Houze 1982; Johnson 1984). For example, during the latter stages of the December 1992 westerly wind burst, negative $Q_2$ was common below 600 hPa (Lin and Johnson 1996b), suggesting the frequent occurrence of stratiform precipitation at that time. In addition, there is some contribution to negative values of $Q_2$ in the lowest 2 km from shallow cumulus clouds and subcloud-layer eddies during nonprecipitating periods of the IOP (Johnson and Lin 1997). There is some hint of a double-peaked structure to $Q_2$ at the largest drying rates in the CFAD, although this structure is not apparent in the mean $Q_2$ profile. Johnson et al. (1996) noted that in deep convection over the warm pool the often-observed double-peaked $Q_2$ profiles, with a minimum near the melting level, can be explained by an inflection in the specific humidity profile in the Tropics that can be traced directly or indirectly to the effects of melting.

The mean $Q_1$ profile in Fig. 3, with a peak of 4°C day$^{-1}$ near 400 hPa, agrees well with the IFA profile presented by Frank et al. (1996) based on a line-integral technique. It also closely resembles the mean heating profiles reported in tropical western Pacific budget studies (Reed and Recker 1971; Nitta 1972; Yanai et al. 1973). In contrast, the $Q_2$ profile for the IFA differs considerably from the earlier western Pacific budget studies, as noted by Lin and Johnson (1996b). In particular, there are negative values of $Q_2$ below 900 hPa. Johnson and Lin (1997) explained this anomalous structure by showing that, although low-level positive values

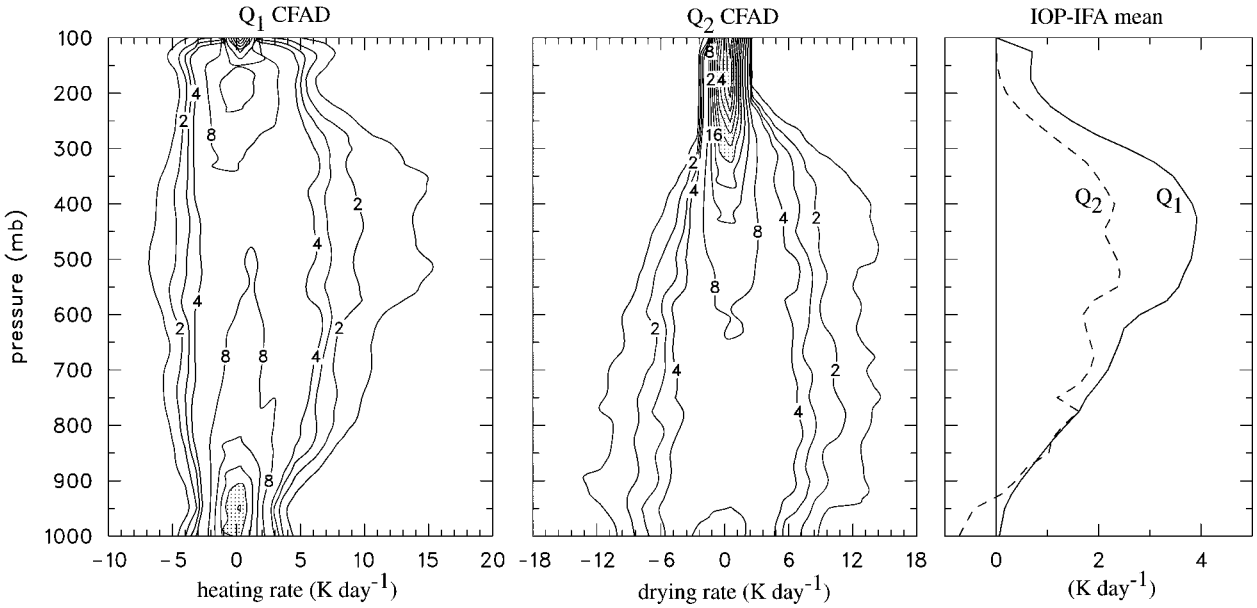


FIG. 3. (left) Contoured frequency by altitude diagrams (CFADs) of (left) IFA-mean apparent heat source $Q_1$ and (center) apparent moisture sink $Q_2$ for COARE IOP; (right) IOP–IFA-mean profiles of $Q_1$ and $Q_2$. CFAD contour interval: 1% for values $<4\%$ and 4% above. Values $>20\%$ are stippled.

of $Q_2$ are commonplace at times of deep convection, nonprecipitating periods with negative $Q_2$ (due to low-level moistening by boundary layer eddies and shallow cumulus) were frequent enough to produce a negative low-level $Q_2$ in the mean. Frank et al. (1996) also show negative $Q_2$ below 900 hPa, but their peak amplitude (near 600 hPa) is about 1°C day$^{-1}$ greater than ours. This difference is likely related to different analysis schemes, the use by Frank et al. of mandatory-level sounding data only, and differing treatment of periods (35 total days) when IFA-perimeter ships *Kexue 1* and *Shiyan 3* were off station.

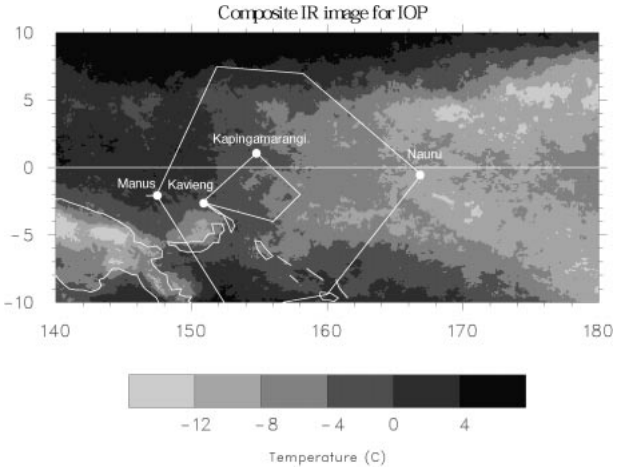


FIG. 4. IOP-mean GMS brightness temperatures (°C) over COARE LSA. Sites with tipping bucket rain gauges are indicated.

## 4. Rainfall estimates

### *a. Comparisons with TOGA–MIT radar results*

Comparison of rainfall estimates from different platforms, for example, radars, satellites, budgets, etc., is a difficult task owing to the different timescales and space scales and error characteristics of the various measurement techniques. To provide a general background within which the various results may be interpreted, we first refer to the IOP-mean distribution of IR brightness temperatures over the COARE large-scale array (LSA) (Fig. 4). Three prominent regions of convection can be inferred from Fig. 4: along 4°N east of 165°E, southeast of the OSA along the South Pacific convergence zone, and over the islands of Papua New Guinea and New Britain (along 5°S west of 152°E). Figure 4 suggests a minimum of rainfall to the west of the IFA, with the IFA itself exhibiting a west-to-east increase in precipitation.

Time series of daily rainfall from tipping bucket (TBG) and optical (ORG) rain gauges at six sites within the COARE domain of Fig. 4 are shown in Fig. 5. The records at Kapingamarangi (a small atoll), *Kexue 1, Shiyan 3,* and Nauru (a small island) suggest significant modulations of rainfall on a monthly timescale in association with the Madden–Julian oscillation (MJO; Madden and Julian 1971). Rainfall time series for sites on larger landmasses (Manus and Kavieng) exhibit more frequent (nearly daily) rainfall in association with sea breeze circulations at those locations. The IOP-mean rainfall amounts in Fig. 5 at the sites with nearly complete records (all but the ships) generally increase from

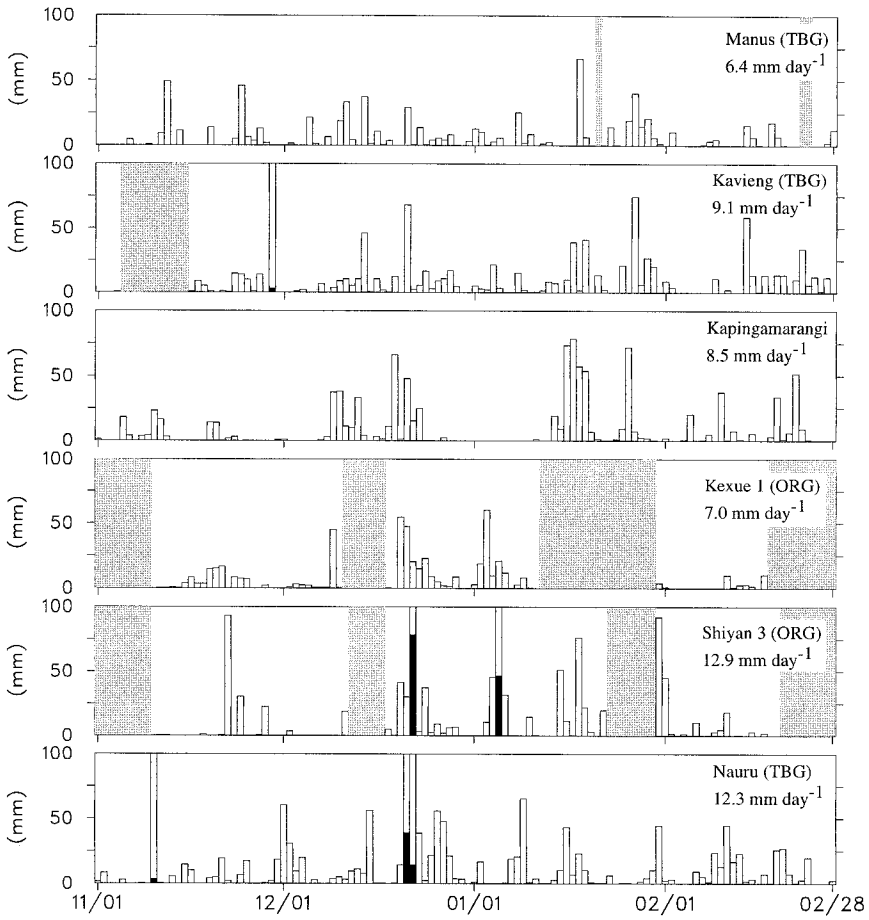


FIG. 5. Time series of daily TBG and ORG measurements for COARE IOP. IOP means for periods when data were available are indicated in upper right. Light shading indicates periods of missing data. Dark shading indicates values in excess of 100 mm.

west to east, consistent with the precipitation pattern inferred from Fig. 4.

The TBG measurements are used to assess the performance of the MQD and Barnes objective analysis schemes. The point measurements of rainfall at Kapingamarangi, Kavieng, Manus, and Nauru are shown in Table 1 along with means for the same periods for the CMAP analysis, the MQD and Barnes scheme, and the NCEP and ECMWF reanalyses at grid points nearest each site. For all stations agreement between observed (TBG) and analyzed rainfall for this four-month period is better for the MQD scheme than the Barnes scheme. Also, note that the MQD estimates are better for IFA sites Kapingamarangi and Kavieng where sonde data coverage is greatest. CMAP and TBG agree reasonably well, but CMAP is based in part upon gauge values so the two are not completely independent. The MQD estimates are also better than the NCEP and ECMWF reanalysis results for the majority of the sites.

Additional results from the two objective analysis methods are given in Table 2, which compares the mean rainfall for the 85 days when the ships *Kexue 1* and *Shiyan 3* (constituting the southeast portion of the IFA) were present to average amounts for the 35 days those

TABLE 1. Point measurements of rainfall (mm day$^{-1}$). MQD refers to multiquadric technique and CMAP is the CPC Merged Analysis of Precipitation (Xie and Arkin 1997).

| Site | IOP days | TBG | CMAP | MQD | Barnes | NCEP | ECMWF |
|---|---|---|---|---|---|---|---|
| Kapinga | 1–120 | 8.5 | 9.6 | 8.4 | 3.4 | 4.8 | 6.8 |
| Kavieng | 15–120 | 9.1 | 9.8 | 10.1 | 7.2 | 5.6 | 6.8 |
| Manus | 1–120 | 6.4 | 7.8 | 4.7 | 3.1 | 5.5 | 4.8 |
| Nauru | 1–120 | 12.3 | 12.9 | 8.6 | 7.1 | 6.0 | 6.0 |
| Average | | 9.1 | 10.0 | 8.0 | 5.2 | 5.5 | 6.1 |

TABLE 2. Budget, satellite, and model rainfall estimates (mm day$^{-1}$). MQD refers to the multiquadric technique, Sat/Mixed to the satellite scheme of Curry et al. (1999), and CMAP to the CPC Merged Analysis of Precipitation (Xie and Arkin 1997). Asterisk (*) refers to values from the GOES Precipitation Index (Arkin and Meisner 1987) for these periods since daily CMAP values are not available. NA means not available.

| Method | IFA; perimeter ships present (85 days) | IFA; perimeter ships not present (35 days) | IFA–IOP | OSA–IOP | LSA–IOP |
|---|---|---|---|---|---|
| MQD | 7.5 | 9.9 | 8.2 | 9.3 | 8.1 |
| Barnes | 5.9 | 5.0 | 5.6 | 9.7 | 7.7 |
| Sat/Mixed | 8.1 | 8.8 | 8.3 | NA | NA |
| CMAP | 10.1* | 12.3* | 9.3 | 9.7 | 9.1 |
| NCEP | 8.5 | 8.1 | 8.4 | 7.6 | 8.3 |
| ECMWF | 7.3 | 5.3 | 6.7 | 7.6 | 8.4 |

ships were off station. It is reasonable to expect that objective analyses and budget-derived rainfall over the IFA should be more reliable for the period when the IFA-perimeter ships were present. The MQD results yield about 30% more rainfall when the ships were off station (9.9 vs 7.5 mm day$^{-1}$), while the Barnes results indicate about 15% less. Results of two independent satellite estimation techniques, the mixed algorithm of Curry et al. (1999) and GPI, indicate an increase in average rainfall during the 35-day period when IFA ships were not present, consistent with the MQD results.[1] This similar behavior of the satellite and MQD estimates provides further support for superiority of the MQD over the Barnes scheme for the COARE IFA region. This conclusion agrees with findings from sensitivity tests by Nuss and Titley (1994), wherein it was shown that for data-sparse fields (such as those treated here) the MQD technique produces more reasonable analyses than the Barnes scheme.

It is noteworthy that for the 85-day period when the IFA-perimeter ships were present, the rainfall estimates from the MQD and Barnes schemes are in reasonable agreement (Table 2). For the entire IOP they agree very well on the larger scales of the OSA and LSA. However, there is large disagreement (9.9 mm day$^{-1}$ for MQD vs 5.0 mm day$^{-1}$ for Barnes) when rainfall is computed for the IFA area when the IFA-perimeter ships were not present. This behavior is illustrated in Fig. 6, where it can be seen that the discrepancy in rain estimates between the two techniques is large for three of the four periods when IFA-perimeter ships were off station. Namely, the two schemes tend to produce markedly different analyses over the IFA when large data voids exist.

Consequently, when entire IOP averages are considered, there is large disagreement between the Barnes 5.6 mm day$^{-1}$ (cited in Lin and Johnson 1996b) and MQD

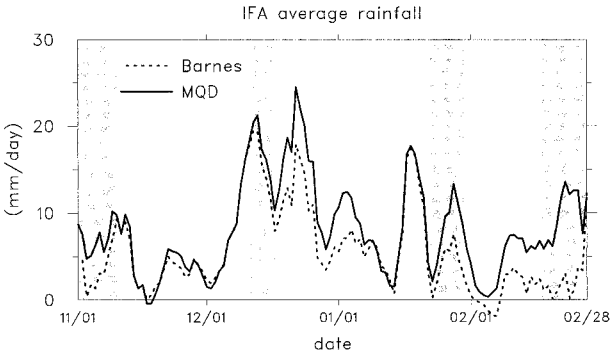


FIG. 6. Time series of IFA-average rainfall (mm day$^{-1}$) for MQD and Barnes techniques for COARE IOP. Rates have been smoothed with a 5-day running mean filter. Shading indicates periods when IFA-perimeter ships were off station.

8.2 mm day$^{-1}$.[2] However, the MQD 8.2 mm day$^{-1}$ is in good agreement with the 9.1 mm day$^{-1}$ estimate by Frank et al. (1996) from the heat budget (following application of the correction suggested in their appendix). It agrees less well with the 10.3 mm day$^{-1}$ that Frank et al. (1996) obtained from the moisture budget; however, as those authors note, their estimate of $E$ in (2) to compute $P$ is ~20% high for the IFA. Compared to the satellite estimates, the IOP-mean budget result of 8.2 mm day$^{-1}$ is almost identical to the 8.3 mm day$^{-1}$ determined by the mixed algorithm of Curry et al. (1999), but somewhat less than that of the CMAP. The 8.2 and 8.3 mm day$^{-1}$ estimates from this study and Curry et al. (1999), respectively, are also in very good agreement with the R/V *Wecoma* three-cruise-mean rainfall rate of 8 mm day$^{-1}$ from Feng et al. (1998) determined as a residual of measured values of evap-

[1] Ebert and Manton (1998) note that the GPI algorithm overestimates radar-derived precipitation amount; nevertheless, it still shows a 22% increase in rainfall when the IFA ships were off station.

[2] In order to test the sensitivity of the budgets to rawinsonde humidity errors, the MQD analysis was rerun using a preliminary humidity correction scheme based on Lucas and Zipser (2000). This correction increased the IOP–IFA-averaged rainfall to 8.4 mm day$^{-1}$ (i.e., by 2.5%). The effect of this correction is to decrease the low-level horizontal advection of dry air over the IFA, which reduces the amplitude of negative $Q_2$ (moistening) in the boundary layer.

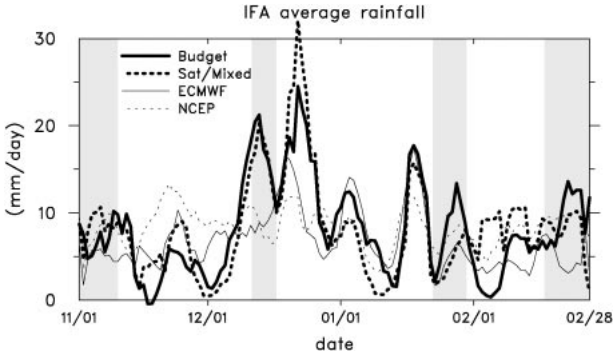


FIG. 7. Time series of IFA-average rainfall (mm day$^{-1}$) for atmospheric (MQD) budget, Curry et al. (1999) mixed satellite algorithm, ECMWF reanalysis, and NCEP reanalysis. Rates have been smoothed with a 5-day running-mean filter. Shading indicates periods when IFA-perimeter ships were off station.

oration and a salinity budget of the ocean mixed layer. The NCEP reanalysis tends to produce about the same amount of rainfall over all of the areas at all times, as also noted by Lau et al. (1996). It agrees quite well with MQD for the IFA and LSA, as do the results for ECMWF. While the IFA–IOP-mean NCEP value of 8.4 mm day$^{-1}$ agrees well with MQD, ECMWF is somewhat less (6.7 mm day$^{-1}$). The difference between the MQD and Barnes IFA–IOP-mean values is significant at the 95% confidence level: all other differences with MQD are not significant at this level.

A comparison of daily rainfall rates (5-day running means) derived from the mixed satellite algorithm of Curry et al. (1999), the MQD budget, NCEP, and ECMWF reanalyses is shown in Fig. 7. As mentioned earlier, on short timescales ($\sim$hours to day) the neglect of cloud storage can have a noticeable effect on the moisture budget. Also, Mapes (1998) has shown that the dispersion of gravity waves by a heat source characteristic of tropical convection can lead to complications in diagnosing the heating ($Q_1$) from coarse rawinsonde arrays. Nevertheless, Fig. 7 shows close agreement between the Curry et al. algorithm and MQD. The two time series track remarkably close to each other, especially during heavy precipitation events. Correlation of daily values is 0.72 (a value of 0.21 is significant at the 99% level). Correlations between budget and ECMWF and NCEP daily values are much less, 0.39 and 0.30, respectively, but are still significant.

The east–west gradient of inferred IFA rainfall in Fig. 4 is supported by the IOP-mean distribution of precipitation derived from the moisture budget using the MQD scheme (Fig. 8a): $<$7 mm day$^{-1}$ northwest of the IFA to $>$14 mm day$^{-1}$ to the southeast. A local minimum of rainfall over the IFA, hinted at in the satellite data (Fig. 4), is much more prominent in the MQD analysis. The Curry et al. satellite algorithm and CMAP (not shown) also indicate an approximately north–south axis of minimum rainfall over the IFA, but their analyses show this axis shifted 1°–2° farther west. Also, the sat-

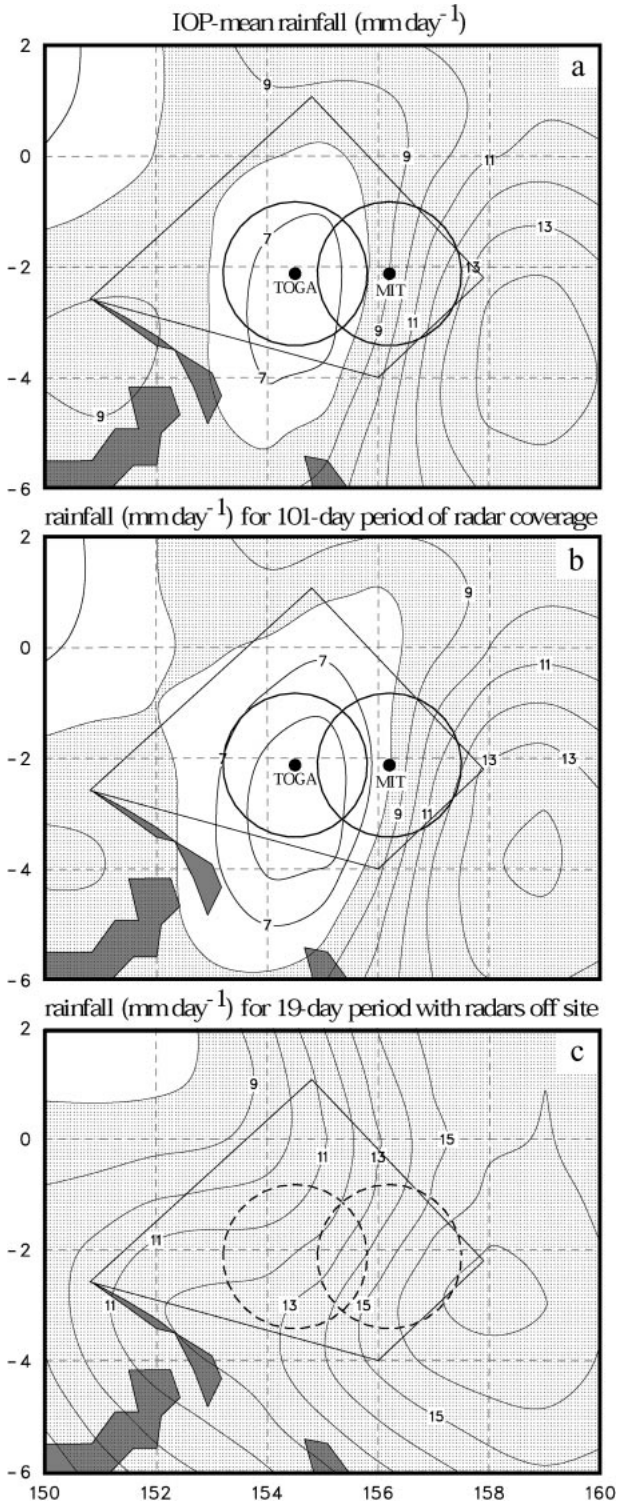


FIG. 8. Moisture-budget-derived precipitation rates (mm day$^{-1}$) for (a) entire IOP, (b) 101-day period of radar coverage, and (c) 19-day period when radars were not operating. Stippling indicates values in excess of 8 mm day$^{-1}$ and dark shading indicates islands. Also shown are nominal deployment positions of the TOGA and MIT radars and their 145-km rain-mapping range rings during the COARE IOP.

TABLE 3. Rainfall estimates (mm day$^{-1}$) during COARE IOP based on atmospheric moisture budget (MQD technique) averaged over the MIT–TOGA radar area (1°–3°S, 153°–157°E) and ship-based radar data (Short et al. 1997).

| Cruise | Number of days | IOP days | MIT–TOGA radar rainfall | Budget rainfall (radar area) | Budget rainfall (IFA area) |
|---|---|---|---|---|---|
| 1 | 35 | 6–40 | 3.8 | 4.7 | 5.2 |
| 2 | 35 | 45–79 | 7.4 | 10.8 | 11.1 |
| 3 | 31 | 84–114 | 4.3 | 4.9 | 5.6 |
| Total/ Average | 101 | | 5.4 | 6.8 | 7.4 |

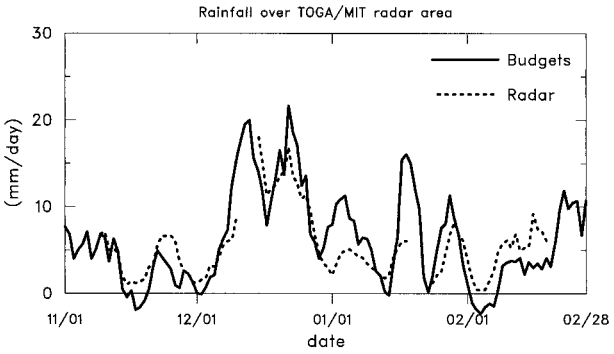


FIG. 9. Time series of 5-day running mean rainfall (mm day$^{-1}$) averaged over the TOGA/MIT radar area for two independent techniques: atmospheric (MQD) budget and ship-based radar (Short et al. 1997).

ellite-based results suggest that the east–west gradient in objectively analyzed rainfall rates over the eastern part of the IFA (Fig. 8a) may be somewhat excessive. The rainfall maximum over New Britain suggested by IR brightness data (Fig. 4) is not evident in the budget analysis due to the lack of sounding data in the vicinity of this island. However, this discrepancy may be exaggerated since, as noted by Frank et al. (1996), convection over large islands in the COARE region (e.g., New Guinea) produced about twice as much high cloud amount per unit of budget rainfall as that over open oceans.

In Table 3 MQD moisture budget rainfall rates are compared to those derived from radar. The radar ship schedules were staggered, so there was radar coverage for 101 out of 120 days in the IOP. Precipitation rates from the moisture budget were averaged over the grid points (1°–3°S, 153°–157°E) that fell within the rain-mapping areas for the 101 days. The average rain rates from the radars [5.4 mm day$^{-1}$, after a 12% correction for range dependence following Short et al. (1997)] and the moisture budget (6.8 mm day$^{-1}$) are in reasonable agreement, although comparisons for the individual cruises suggest the discrepancy is systematic. For the same time period and same area, the Curry et al. (1999) satellite algorithm gives 8.0 mm day$^{-1}$. These three estimates span a considerable range, but considering the uncertainties in radar rainfall estimation and the difficulties in interpolating the budget and satellite results to the relatively small radar area, such a disagreement is not too surprising. Despite the differences in the means, time series of the radar and budget results (Fig. 9) indicate a good correlation between these two independent precipitation estimates. The correlation coefficient $r$ for daily averaged values is 0.55 ($r > 0.23$ is significant at the 99% level for this 101-day period).

Figure 8b shows the rainfall distribution for the 101-day period of the radar deployments. The distribution generally resembles that of the 120-day IOP (Fig. 8a); however, a map of the rainfall for the 19-day period with radars off site (Fig. 8c) shows higher amounts over the IFA during that time. This result is consistent with the finding (Table 3) that the radar cruise-period mean IFA budget rainfall, 7.4 mm day$^{-1}$, is less than the IOP-mean IFA budget rainfall (8.2 mm day$^{-1}$, Table 2). It is also consistent with satellite estimates from Curry et al. (1999), which indicate an IFA-mean rainfall rate of 8.0 mm day$^{-1}$ when the radar ships were deployed and 12.1 mm day$^{-1}$ when they were off station. These results indicate that the 101-day deployment of the radars was on average during a relatively dry period of the IOP.

### *b. Comparisons with NCEP and ECMWF reanalyses*

Table 2 shows that the IOP-mean NCEP and ECMWF reanalysis rainfall rates for the OSA (7.6 mm day$^{-1}$) are about 20% less than that from MQD (9.3 mm day$^{-1}$). A plot of the zonal-average rainfall rate from 150° to 160°E (the approximate longitudes of the OSA) reveals that at individual latitudes there are large discrepancies on a monthly basis for both reanalyses (Fig. 10). A striking difference, however, between the NCEP, ECMWF, and MQD results is the persistent wet biases of the two reanalyses between 5° and 10°N and dry biases near the equator. A similar discrepancy exists between the reanalysis rainfall distributions and the satellite–rain gauge-based CMAP (Fig. 10), the latter generally being consistent with MQD (except for February).

A possible explanation for the excessive NCEP and ECMWF rainfall in the northern ITCZ may be related to the sounding humidity biases described earlier, namely, the moist-biased VIZ measurements between 7° and 13°N and the dry-biased Vaisala measurements elsewhere (Zipser and Johnson 1998). This situation is shown in Fig. 11, a N–S cross section of relative humidity averaged between 150° and 160°E, with positions of VIZ and Vaisala sites indicated at the bottom. Anomalously moist conditions can be seen at low levels and in the upper troposphere between 5° and 15°N, near the indicated positions of the VIZ sensors. It is likely that the convective parameterizations used in the reanalyses translate the high boundary layer moisture into excessive precipitation there. As noted earlier, while the moisture biases have only a small (<3%) impact on the budgets, their effect on numerical model results can be

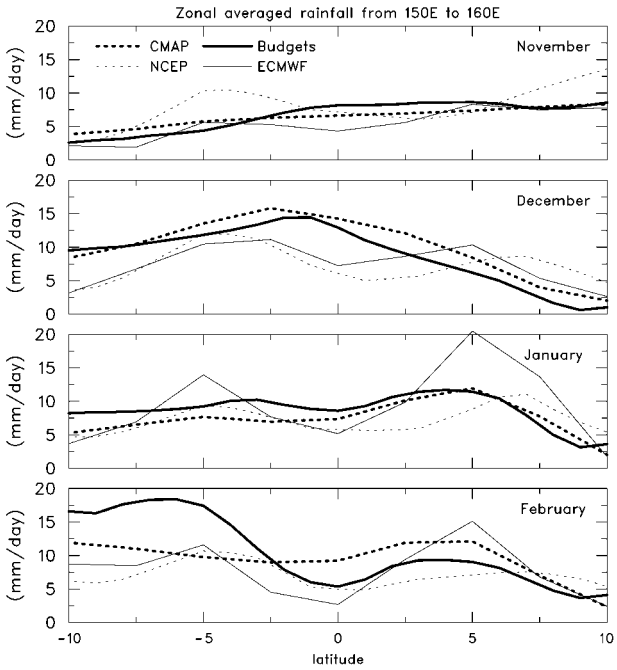


FIG. 10. Zonally averaged rainfall rates (mm day$^{-1}$) between 150° and 160°E for four months for CMAP, NCEP reanalysis, ECMWF reanalysis, and atmospheric budget results based on MQD.

large since the energy available for convection and convective triggering are very sensitive to boundary layer moisture. The ECMWF reanalysis uses the Tiedtke (1989) cloud mass flux scheme, which would be expected to generate more precipitation under moister conditions, all other factors being the same. In the case of the Arakawa–Schubert scheme used in the NCEP reanalysis, excessively moist conditions likely increase the cloud work function, thereby prematurely activating the quasi-equilibrium condition, ultimately leading to more precipitation. In response to the vigorous convection between 3° and 10°N in the NCEP and ECMWF reanalyses, excessive compensating subsidence near the equator, along with the (Vaisala) dry-biased low-level conditions there, may lead to anomalously low NCEP and ECMWF rainfall amounts near the equator (lower panel, Fig. 11).

## 5. Radiative heating rates

The general agreement between moisture budget, radar, and satellite-derived rain rates motivates use of the combined heat and moisture budgets to determine the net tropospheric radiative heating rate $\langle Q_R \rangle$ as a residual. A time series of $\langle Q_R \rangle$ (5-day running mean) computed from (3) is shown in Fig. 12 (middle panel), with high-cloud fractional coverage (cirrus Ci, cirrostratus Cs, and their sum; bottom panel) derived from International Satellite Cloud Climatology Project (ISCCP; Rossow and Schiffer 1991) data. A plot of $\langle Q_R \rangle$ incorporating sonde humidity errors and rainfall effects as discussed in section 2 is also shown in Fig. 12 (thin curve, middle panel), indicating a maximum impact on $\langle Q_R \rangle$ at times of maxiumum rainfall (e.g., December). Here $\langle Q_R \rangle$ undergoes a marked variation throughout the IOP, with greatest cooling generally at times of minimum high cloud cover.[3] For example, in early December $\langle Q_R \rangle$ was about $-1$ K day$^{-1}$, with very little high clouds and precipitation (Fig. 6), as illustrated in the infrared satellite image on 1 December (Fig. 13a). At this time, longwave cooling to space was maximized. In contrast, $\langle Q_R \rangle$ was a minimum, even reverting to a warming, at times of maximum high clouds (the diagnosed warming is reduced slightly by the inclusion of sonde humidity errors and rainfall effects). Late December is an example (Fig. 12), at which time extensive cirrus coverage can be inferred from the IR satellite image for 22 December (Fig. 13b). The net warming is presumably a result of decreased longwave emission from the atmosphere by the upper-level cloud layer. In support of these findings, Stephens et al. (1994) have shown that the cloud longwave forcing over the warm pool and eastern Indian Ocean is greater than other locations around the world. Also, Wong et al. (1993) have demonstrated using a cloud-resolving model of a tropical convective system that during the latter stages of convection, when only an upper-tropospheric mesoscale anvil cloud remains, the atmospheric column experiences radiative heating. The warming is maximized in the upper troposphere between 200 and 300 hPa, where solar heating of the anvil occurs, but also extends to the lower troposphere, where there is infrared heating in proximity to the base of the anvil (Albrecht and Cox 1975; Webster and Stephens 1980).

The upper panel of Fig. 12 shows the temperature deviation $T'$ from the IOP mean as a function of height. Two strong cool anomalies near 100 hPa can be observed in mid-December and late January. Similar ~1-week cool anomalies just below the tropopause (mean tropopause height during these periods was ~90 hPa) have been reported in the equatorial Asian monsoon region by Johnson (1986). They were attributed to possible effects of overshooting by cumulonimbus towers (e.g., Reed 1978) and/or cloud-top radiative cooling (Albrecht and Cox 1975; Webster and Stephens 1980). There are also two prominent warm anomalies (>1 K) in the upper troposphere, one in late December and the other in late January. Upper-tropospheric warming associated with the MJO has also been reported by Hendon and Salby (1994) and Yanai et al. (2000). Yanai et al. (2000) show that the perturbation temperature $T'$ and perturbation heating $Q'$ are positively correlated over

[3] For reasons that are not fully understood, a slight phase shift is seen between the peaks in $\langle Q_R \rangle$ and high cloud amounts. Maximum $\langle Q_R \rangle$ should be expected at times of maximum coverage of optically thin (Ci) clouds, but the prominent Ci peak in late December occurs about 5 days after the peak in $\langle Q_R \rangle$.

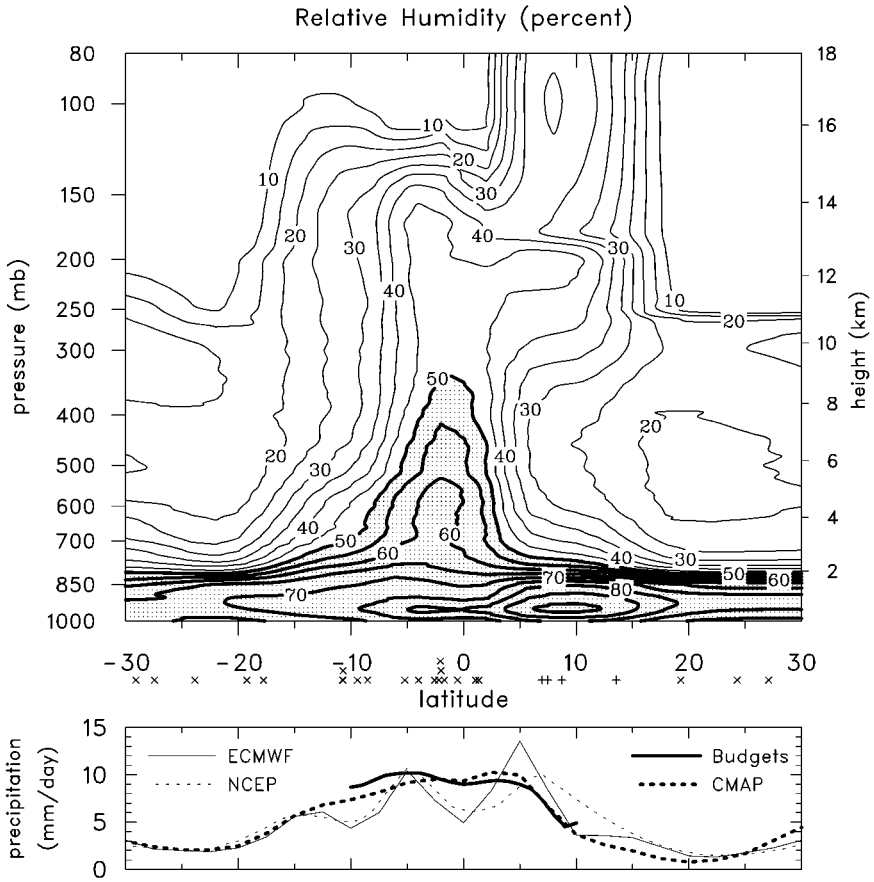


FIG. 11. (upper) IOP-mean zonally averaged relative humidity between 150° and 160°E. Values greater than 50% stippled. Symbols at base of panel indicate the latitudes of Vaisala (×) and VIZ (+) sites used in creating the analysis. (lower) Zonally averaged rainfall rate (mm day$^{-1}$) over same longitude band for NCEP and ECMWF reanalyses, CMAP, and atmospheric budget results based on MQD.

the warm pool, indicating a generation of perturbation available potential energy, which is rdirectly converted to perturbation kinetic energy by positive $w'T'$ correlations.

The time series of $\langle Q_R \rangle$ and $T'$ in Fig. 12 suggests a possible link between the radiative heating and actual warming; however, the interpretation is likely complicated by other factors influencing the temperature field, notably latent heat release and dynamical effects. For example, referring to Figs. 6 and 7, it can be seen that the warm anomalies aloft correspond to periods of greatest precipitation, and hence latent heating, Yanai et al. 2000), as also observed in GATE (e.g., Thompson et al. 1979). Also, Bantzer and Wallace (1996) have used satellite microwave sounding unit data to infer a global-scale upper-tropospheric warming in association with the MJO, which they argue arises in response to sinking accompanying a rapidly eastward-propagating Kelvin wave front generated by latent heat release. However, the typical warmings observed by Bantzer and Wallace are small, (~0.15 K) in relation to those observed over the IFA. Thus, it is possible that radiative heating is contributing, along with other effects, to temperature anomalies over the warm pool.

If the radiative heating in late December is indeed contributing to slight warming aloft at that time, it may then be one of several factors leading to the demise of precipitation toward the end of that month (Fig. 6) by increasing the stability aloft. Of course, another factor operating is the pronounced upper-ocean cooling (e.g., Weller and Anderson 1996) accompanying the strong low-level westerly wind burst in late December, which contributes to a reduction in convective available potential energy.

The large temporal variability in $\langle Q_R \rangle$ in association with the MJO, up to 1.5 K day$^{-1}$ (Fig. 12), as well as variations on shorter timescales, implies large horizontal variability in shortwave plus longwave radiative heating rates over the Pacific. Such variations are likely to have significant impacts on tropical circulations (Webster, 1994). On the scale of mesoscale convective systems or super cloud clusters (Nakazawa 1988), reduced longwave cooling within the cloud system and enhanced cooling outside may invigorate the low-level circulation

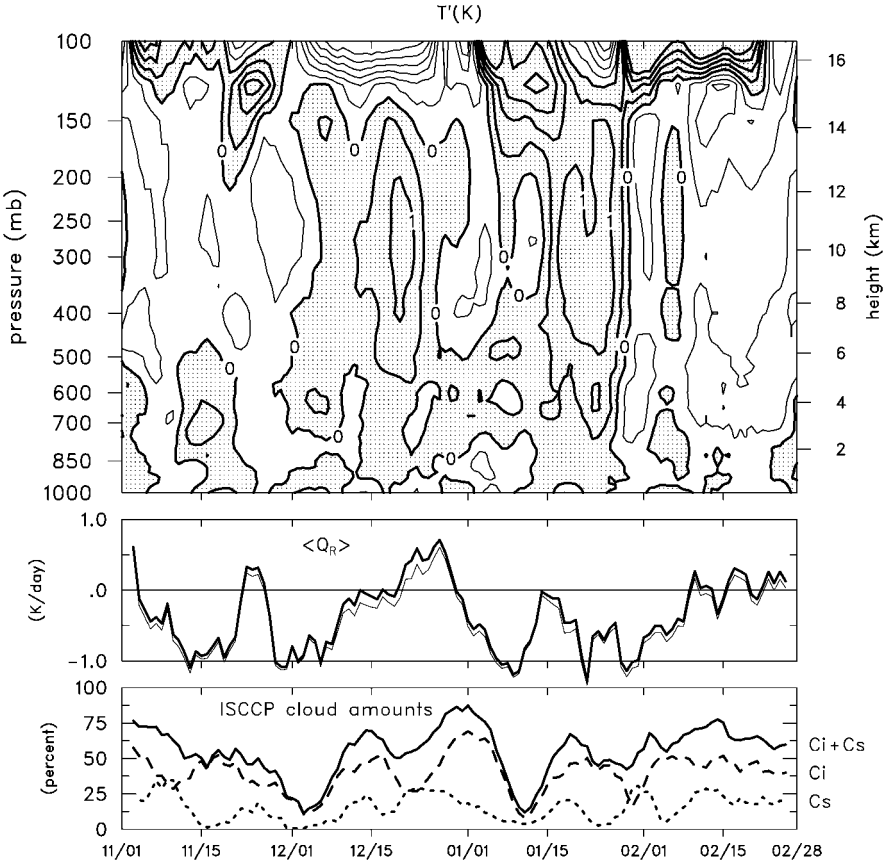


FIG. 12. Time series of IFA-averaged fields (upper) Temperature deviation (contour interval 0.5 K) from IOP mean. Stippling indicates positive deviations. (middle) Net tropospheric radiative heating rate $\langle Q_R \rangle$ (K day$^{-1}$) computed as a budget residual (heavy curve) and $\langle Q_R \rangle$ recomputed to include humidity correction and rainfall effects (thin curve). (lower) ISCCP cirrus (Ci), cirrostratus (Cs), and total high cloud amount (%). All fields have been smoothed with a 5-day running mean filter.

into convection during nighttime hours (e.g., Gray and Jacobson 1977). Slingo and Madden (1991) modeled the effect of cloud longwave forcing on MJO and found minimal effects; however, results are dependent on model parameterizations and the simulation cloud fields. On larger scales, the modulation of the vertical distribution of radiative heating by high-level clouds can affect large-scale tropical circulations. Although our procedure permits diagnosis of the vertical integral of $Q_R$, not its vertical profile, the studies of Albrecht and Cox (1975), Webster and Stephens (1980), and Wong et al. (1993) indicate that upper-tropospheric cloud layers can produce longwave radiative warming near cloud base in the middle to upper troposphere. The resultant modified profile of diabatic heating in the convective area has been shown to have major impacts on the Walker (Hartmann et al. 1984) and Hadley (Raymond 2000) circulations.

IOP-mean radiative heating rates derived from the budgets (uncorrected for humidity biases and effects of rain discussed in section 2a) are shown in Table 4, both for the IFA and the OSA. The mean values of $\langle Q_R \rangle$ for the IFA and OSA are $-0.32$ and $-0.50$ K day$^{-1}$, respectively. The greater cooling rate for the OSA is consistent with the slightly reduced high cloud coverage for this larger area, as inferred from the IR brightness temperature map (Fig. 4).

Comparison of the budget results with estimates from other studies is shown in Table 5. Included with the results of this study are error estimates of $\langle Q_R \rangle$ based on a consideration of the following uncertainties: 1) $\sim$10 W m$^{-2}$ for surface fluxes $S + LE$ over IFA, $\sim$15 W m$^{-2}$ for the OSA; and 2) $\sim$5 W m$^{-2}$ for the vertical advection terms in $\langle Q_1 \rangle - \langle Q_2 \rangle$. The latter is based on the finding of a 5 W m$^{-2}$ difference between $\langle Q_R \rangle$ computed using adjusted and unadjusted values of $\omega$. In addition, the impacts of four effects—the Lucas and Zipser (2000) humidity correction, the effects of rain on the computation of $\omega$, the sensible heat flux due to rain, and frictional dissipation associated with falling rain (the latter following Emanuel and Bister 1996)—enhancing the IOP-mean cooling rate by 0.04, 0.01, 0.02, and 0.02 K day$^{-1}$, respectively, are shown in Table

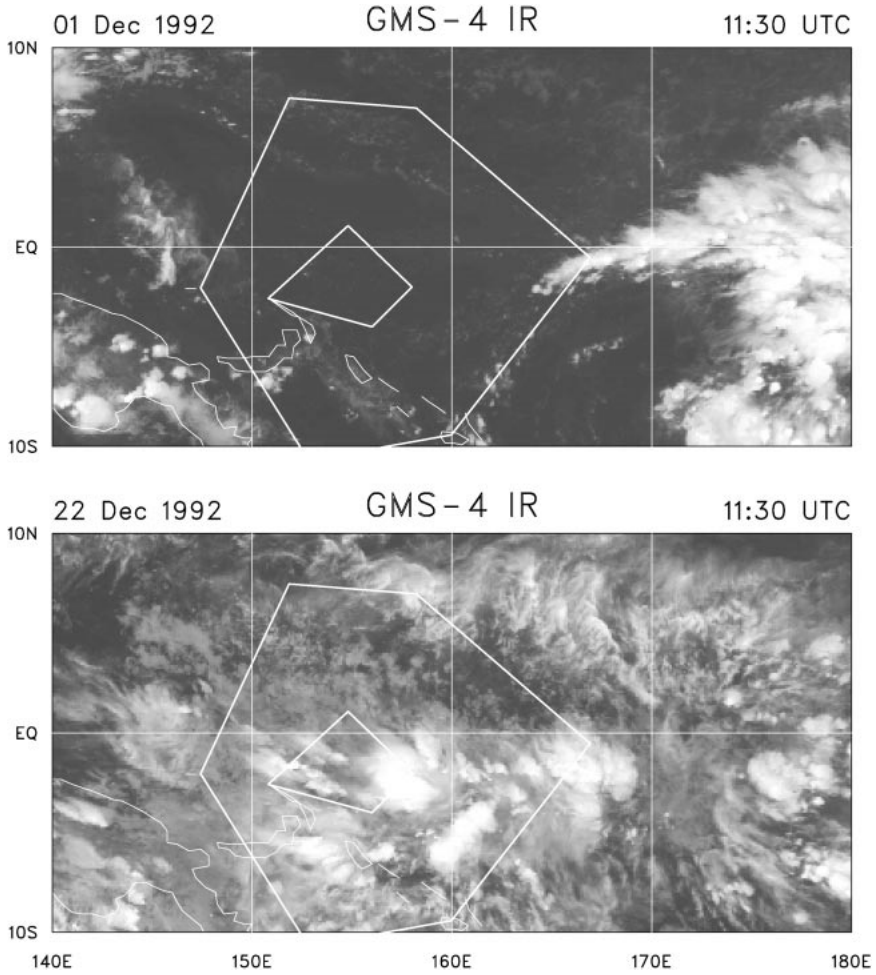


FIG. 13. GMS infrared satellite image for 1130 UTC on (a) 1 Dec and (b) 22 Dec.

5, leading to a IOP–IFA-mean diagnosed $\langle Q_R \rangle$ of $-0.41$ K day$^{-1}$.

The values of $\langle Q_R \rangle$ for this study and Frank et al. (1996) are in reasonably good agreement, considering the different data resolutions and methodologies employed. The most striking aspect of the COARE results is their large disagreement with oft-quoted tropical radiative heating rates. For example, the COARE results are nearly half the clear-sky Dopplick (1972) value of $-1.1$ K day$^{-1}$. Naturally, with cloud cover the COARE $\langle Q_R \rangle$ should be less than clear-sky estimates. However, they are still less than the all-sky (full range of cloud conditions) GATE value of $-1.1$ K day$^{-1}$ from Cox and Griffith (1979) and the heat-budget residual $-0.9$ K day$^{-1}$ from Thompson et al. (1979). They are even considerably smaller than the Cox and Griffith (1979) GATE convectively disturbed (day 245) value of $-0.8$ K day$^{-1}$. The COARE atmospheric budget results do, however, fall within the ranges of various independent estimates for the COARE IFA based on measurements and radiation models with assumed moisture and cloud distributions: $-0.44$ K day$^{-1}$ from T. Ackerman (cited in Frank et al. 1996); $-0.46$ K day$^{-1}$ based on Chou et al. (1998) (M.-D. Chou 1999, personal communication); $-0.84$ K day$^{-1}$ based on Curry et al. (1999) (W. Rossow and Y.-C. Zhang 1999, personal communication). Although the agreement between the budget results and several of these estimates is gratifying, the large range of values reflects the continuing uncertainty in determining radiative heating rates in the Tropics under the full range of cloudiness conditions.

Recent claims by Cess et al. (1995), Ramanathan et

TABLE 4. Integrated budget results for IFA and OSA (neglecting corrections for sounding humidity biases and rain effects as discussed in text) (1 K day$^{-1}$ $\simeq$ 108 W m$^{-2}$).

| Units | $\langle Q_1 \rangle$ | $-$ | $\langle Q_2 \rangle$ | $=$ | $\langle Q_R \rangle$ | $+S$ | $+LE$ |
|---|---|---|---|---|---|---|---|
| | | | IOP–IFA averages | | | | |
| W m$^{-2}$ | 211 | | 131 | | ($-35$) | 9 | 106 |
| K day$^{-1}$ | 1.95 | | 1.21 | | ($-0.32$) | | |
| | | | IOP–OSA averages | | | | |
| W m$^{-2}$ | 213 | | 152 | | ($-54$) | 8 | 107 |
| K day$^{-1}$ | 1.97 | | 1.41 | | ($-0.50$) | | |

TABLE 5. Comparison of radiation estimates for the Tropics. COARE estimates are for the IOP. Here M + M signifies measurements and radiation models with assumed moisture and cloud distributions.

| Region | Conditions | Source | Method | Net radiation (K day$^{-1}$) |
|---|---|---|---|---|
| COARE OSA | All sky | Frank et al. (1996) | Atmospheric budgets | −0.65* |
| COARE IFA | All sky | Frank et al. (1996) | Atmospheric budgets | −0.62* |
| COARE OSA | All sky | This study | Atmospheric budgets | −0.50 ± 0.20 |
| COARE IFA | All sky | This study | Atmospheric budgets | −0.32 ± 0.15 |
| COARE IFA | All sky | This study** | Atmospheric budgets | −0.41 ± 0.15 |
| COARE IFA | All sky | Rossow–Zhang (based on Curry et al. 1999) | M + M | −0.84 |
| COARE IFA | All sky | T. Ackerman (cited in Frank et al. 1996) | M + M | −0.44 |
| COARE IFA | All sky | Chou (based on Chou et al. 1998) | M + M | −0.46 |
| GATE | Cloudy to clear | Cox and Griffith (1979) | M + M | −0.8 to −1.1 |
| GATE | All sky | Thompson et al. (1979) | Atmospheric budgets | −0.9 |
| Tropics | Clear sky | Dopplick (1972) | M + M | −1.1 |

* Based on R/V *Moana Wave* surface flux data.

** Includes Lucas and Zipser (2000) humidity correction, effects of rain on computation of $\omega$, sensible heat flux due to rain, and frictional dissipation by falling rain (Emanuel and Bister 1996).

al. (1995), and Pilewskie and Valero (1995) of anomalous absorption by tropical cirrus appear to be consistent with the small cooling rates derived from the budgets. However, caution must be exercised in drawing any conclusions from this evidence since the smaller cooling rates may simply be an indication of greater cloud longwave forcing over the warm pool, as recently shown by Stephens et al. (1994) and Bergman and Hendon (1998). Clearly, more work is needed to understand the causes of the observed values of $\langle Q_R \rangle$ and reconcile the differences in estimates between the various studies.

## 6. Summary and conclusions

An important objective of TOGA COARE was the determination of precipitation rates over the warm pool using various approaches: rain gauges, remote sensing (radars, satellites, atmospheric profilers), atmospheric budgets, upper-ocean budgets, and numerical modeling. In this study, rainfall rates for the COARE Intensive Flux Array (IFA) have been computed from the atmospheric moisture budget and compared to estimates from other studies. Particular attention is focused on comparisons with independent rainfall estimates from the shipboard MIT and TOGA radars. Using the COARE bulk flux algorithm (Fairall et al. 1996) to estimate surface evaporation over the IFA, the IFA moisture budget-derived average rainfall for the 120-day intensive observing period (IOP) is 8.2 mm day$^{-1}$. However, for a smaller area within the IFA containing the rain-mapping domain of the TOGA and MIT radars, the atmospheric budget for the 101-day radar deployment yields a smaller value, 6.8 mm day$^{-1}$. This value is slightly greater than the radar range-corrected rainrate estimate from Short et al. (1997) of 5.4 mm day$^{-1}$. The radar-cruise-period mean IFA budget rainfall rate, 7.3 mm day$^{-1}$, is less than the IOP-mean IFA budget rainfall (8.2 mm day$^{-1}$), indicating that *the 101-day deployment of the radars was during a relatively dry period of the IOP*. The budget IFA–IOP estimate of 8.2 mm day$^{-1}$ is in very good agreement with three independent rainfall estimates: 1) 8.3 mm day$^{-1}$ from the mixed microwave–visible–infrared satellite algorithm of Curry et al. (1999), 2) 9.3 mm day$^{-1}$ from the CPC Merged Analysis of Precipitation of Xie and Arkin (1997), and 3) 8 mm day$^{-1}$ from the ocean salinity budget (Feng et al. 1998).

Rainfall rates have also been compared to those obtained from the NCEP and ECMWF reanalyses (Kalnay et al. 1996; Gibson et al. 1997). The most striking difference between the budget and NCEP results is a persistent wet bias of the reanalyses between 5° and 10°N and a dry bias near the equator. A possible explanation for these discrepancies is related to biases associated with the sounding humidity sensors, namely, excessively moist VIZ measurements between 7° and 13°N and dry-biased Vaisala measurements elsewhere (Zipser and Johnson 1998; Lucas and Zipser 2000). It is likely that the convective parameterizations used in the reanalyses translate the high boundary layer moisture near 10°N into excessive precipitation there. Although these sounding moisture biases have only a small effect on the budgets (<3%), their effect on numerical model results can be large since available energy for convection and convective triggering are very sensitive to boundary layer moisture. In response to the vigorous convection between 5° and 10°N in the reanalyses, excessive compensating subsidence near the equator, along with the (Vaisala) dry-biased low-level conditions there, leads to anomalously low reanalysis rainfall amounts near the equator.

Computations of the vertically integrated net radiative heating rate $\langle Q_R \rangle$ as a residual from the heat and moisture budgets yield a IOP-mean value of −0.32 K day$^{-1}$ for the IFA and −0.50 K day$^{-1}$ for the larger outer

sounding array (OSA). However, when corrected for Vaisala humidity biases, effects of rain on the computation of $\omega$, the sensible heat flux due to rain, and frictional dissipation associated with falling rain, the IOP-mean for the IFA is $-0.41$ K day$^{-1}$. These cooling rates fall within the range of those computed using surface and top-of-the-atmosphere radiation measurements and radiation models: $-0.84$ K day$^{-1}$ based on Curry et al. (1999) (W. Rossow and Y.-C. Zhang 1999, personal communication), $-0.44$ K day$^{-1}$ by Ackerman (cited in Frank et al. 1996), and $-0.46$ K day$^{-1}$ based on Chou et al. (1998) (M.-D. Chou 1999, personal communication). A conclusion emerging from this and other studies is that *the net tropospheric radiative cooling rate over the warm pool is considerably smaller than previously cited values for the Tropics* [e.g., clear-sky $-1.1$ K day$^{-1}$, Dopplick (1972); cloudy to clear sky $-0.8$ to $-1.1$ K day$^{-1}$, Cox and Griffith (1979)]. However, the findings are consistent with the those of Stephens et al. (1994) and Bergman and Hendon (1998) of greater cloud longwave forcing over the western Pacific and Indian Oceans than other areas of the Tropics. The cooling rates not appear small enough to require invoking anomalous shortwave absorption by tropical cirrus as proposed by Cess et al. (1995), Ramanathan et al. (1995), and Pilewskie and Valero (1995), since some of the radiation-based estimates of $\langle Q_R \rangle$ agree favorably with the atmospheric budget results without any assumption of anomalous absorption. This finding appears to support the conclusion of Stephens (1996) that evidence to date for the anomalous absorption hypothesis is far from conclusive.

Time series of $\langle Q_R \rangle$ indicate certain periods during the IOP up to a week long (e.g., late December) when a net radiative warming of the troposphere is observed. These periods correspond to times of abundant high-level clouds. There is evidence from cloud modeling studies that such warming can occur as a combined effect of solar heating of mesoscale anvil-type clouds in the upper troposphere and infrared heating in proximity to their bases (Wong et al. 1993). This upper-tropospheric warming, leading to stabilization, may be one of the factors leading to the demise of convection in the latter stages of westerly wind bursts, when strong upper-tropospheric easterlies spread cirrus over expansive areas of the warm pool as the convectively active portion of the Madden–Julian oscillation (MJO) moves eastward toward the date line. The temporal variation of $\langle Q_R \rangle$ on the timescale of the MJO is found to be large, up to $\sim 1.5$ K day$^{-1}$. The implied horizontal variation of $\langle Q_R \rangle$ is large enough to have significant impacts on the tropical Walker and Hadley circulations (Hartmann et al. 1984; Slingo and Slingo 1988, 1991; Randall et al. 1989; Sherwood et al. 1994; Webster 1994; Raymond 2000).

The good overall agreement between atmospheric moisture budget–derived rainfall rates and those from shipboard radars, the satellite algorithms of Curry et al. (1999) and Xie and Arkin (1997), and ocean salinity budget of Feng et al. (1998), lends credence to the computations of IOP-mean net radiative heating rate as a residual from the budgets. Nevertheless, caution must be exercised in extrapolating the IOP-mean results for the COARE IFA too generally. For example, Frank et al. (1996) found considerable regional variability in the budget residuals across the western Pacific. Part of this variability may be due to the sparseness of data outside the IFA. In addition, Lukas et al. (1995) note that the COARE IOP took place during a period when the maximum rainfall was displaced eastward from its normal position (to around 170°E) in association with the revival of ENSO conditions during the second half of the IOP. Finally, considering the rather large spread (up to 0.4 K day$^{-1}$) in $\langle Q_R \rangle$ determined from radiation models and assumed cloud distributions, further work is clearly needed to reduce the uncertainty of net radiative heating rate estimates in the Tropics.

*Acknowledgments.* This research has been supported by the National Oceanic and Atmospheric Administration, under Grants NA37RJ0202 and NA67RJ0152. The authors acknowledge helpful discussions with Ming-Dah Chou, Judy Curry, Kerry Emanuel, Roger Lukas, Brian Mapes, Dave Raymond, Bill Rossow, Wayne Schubert, Julia Slingo, Graeme Stephens, Kevin Trenberth, Peter Webster, and Yuanchong Zhang; the comments of two anonymous reviewers; the assistance of Rick Taft with figures; and the provision of satellite data by Tetsuo Nakazawa.

## APPENDIX

### Parameter Specification in the Multiquadric Technique

The multiquadric interpolation scheme used in this study (Nuss and Titley 1994) has three free parameters that need to be specified, which determine the characteristics of the interpolation. Though our choice for the specific values of these parameters may not be optimal for a given data distribution, their selection resulted in consistently accurate and reasonable-looking analyses. The first of these is the smoothing parameter $\lambda$, which determines the amount of spectral low-pass filtering. Increasing the value of this parameter produces analyses with fewer small-scale features. The next parameter, referred to as the multiquadric parameter ($c$), determines the curvature of the hyperboloids used in the interpolation but in practice is necessary for computational stability when solving the equation system implicit in the MQD scheme. By experimentation, we determined that dimensional values of $\lambda = 0.0025$ and $c = 0.2$ produced the best overall fit to the data (i.e., resolved small-scale features in data-dense regions without introducing spurious noise in data-sparse regions). The final parameter, $\sigma$, accounts for observational uncer-

tainity and is specified based on the quality of the data type. For the analysis of the fields of surface pressure, height, temperature, wind, and specific humidity we chose $\sigma$ to be 1 hPa, 10 m, 0.5°C, 2 m $s^{-1}$ and 1 g $kg^{-1}$, respectively.

## REFERENCES


Albrecht, B. A., and S. K. Cox, 1975: The large-scale response of the tropical atmosphere to cloud modulated infrared heating. *J. Atmos. Sci.,* **32,** 16–24.

Arkin, P. A., and B. N. Meisner, 1987: The relationship between large-scale convective rainfall and cold cloud over the western hemisphere during 1982–1984. *Mon. Wea. Rev.,* **115,** 51–74.

Bantzer, C. H., and J. M. Wallace, 1996: Intraseasonal variability in tropical mean temperature and precipitation and their relation to the tropical 40–50 day oscillation. *J. Atmos. Sci.,* **53,** 3032–3045.

Barnes, S. L., 1964: A technique for maximizing details in numerical weather map analysis. *J. Appl. Meteor.,* **3,** 396–409.

——, 1973: Mesoscale objective map analysis using weighted time-series observations. NOAA Tech. Memo. ERL NSSL-62, 60 pp. [NTIS COM-73-10781.]

Bergman, J. W., and H. H. Hendon, 1998: Calculating monthly radiative fluxes and heating rates from monthly cloud observations. *J. Atmos. Sci.,* **55,** 3471–3491.

Betts, A. K., 1974: Further comments on ''A comparison of the equivalent potential temperature and the static energy.'' *J. Atmos. Sci.,* **31,** 1713–1715.

Cess, R. D., and Coauthors, 1995: Absorption of solar radiation by clouds: Observations versus models. *Science,* **267,** 496–499.

Chou, M.-D., W. Zhao, and S.-H. Chou, 1998: Radiation budgets and cloud radiative forcing in the Pacific warm pool during TOGA COARE. *J. Geophys. Res.,* **103,** 16 967–16 977.

Ciesielski, P. E., L. M. Hartten, and R. H. Johnson 1997: Impacts of merging profiler and rawinsonde winds on TOGA COARE analyses. *J. Atmos. Oceanic Technol.,* **14,** 1264–1279.

Cox, S. K., and K. T. Griffith, 1979: Estimates of radiative divergence during Phase III of the GARP Atlantic Tropical Experiment. Part II: Analysis of Phase III results. *J. Atmos. Sci.,* **36,** 586–601.

Curry, J. A., C. A. Clayson, W. B. Rossow, R. Reeder, Y.-C. Zhang, P. J. Webster, G. Liu, and R.-S. Sheu, 1999: High-resolution satellite-derived dataset of the surface fluxes of heat, freshwater, and momentum for the TOGA COARE IOP. *Bull. Amer. Meteor. Soc.,* **80,** 2059–2080.

Dopplick, T. G., 1972: Radiative heating of the global atmosphere. *J. Atmos. Sci.,* **29,** 1278–1294.

Ebert, E. E., and M. J. Manton, 1998: Performance of satellite rainfall estimation algorithms during TOGA COARE. *J. Atmos. Sci.,* **55,** 1537–1557.

Emanuel, K. A., and M. Bister, 1996: Moist convective velocity and buoyancy scales. *J. Atmos. Sci.,* **53,** 3276–3285.

——, and M. Živković-Rothman, 1999: Development and evaluation of a convection scheme for use in climate models. *J. Atmos. Sci.,* **56,** 1766–1782.

Fairall, C. W., E. F. Bradley, D. P. Rogers, J. B. Edson, and G. S. Young, 1996: Bulk parameterization of air-sea fluxes for TOGA COARE. *J. Geophys. Res.,* **101** (C2), 3747–3764.

Feng, M., P. Hacker, and R. Lukas, 1998: Upper ocean heat and salt balances in response to a westerly wind burst in the western equatorial Pacific during TOGA COARE. *J. Geophys. Res.,* **103,** 10 289–10 311.

Frank, W. M., H. Wang, and J. L. McBride, 1996: Rawinsonde budget analyses during the TOGA COARE IOP. *J. Atmos. Sci.,* **53,** 1761–1780.

Gibson, J. K., P. Kallberg, S. Uppala, A. Hernandez, A. Nomura, and E. Serrano, 1997: ERA description. ECMWF Re-Analysis Project Rep. Series 1, European Centre for Medium-Range Weather Forecasts, 72 pp.

Godfrey, J. S., R. A. Houze Jr., R. H. Johnson, R. Lukas, J.-L. Redelsperger, A. Sumi, and R. Weller, 1998: The Coupled Ocean Atmosphere Response Experiment (COARE): An interim report. *J. Geophys. Res.,* **103,** 14 395–14 450.

Gosnell, R., C. W. Fairall, and P. J. Webster, 1995: The sensible heat of rainfall in the tropical ocean. *J. Geophys. Res.,* **100,** 18 437–18 442.

Gray, W. M., and R. W. Jacobson Jr., 1977: Diurnal variation of oceanic deep cumulus convection. *Mon. Wea. Rev.,* **105,** 1171–1188.

Harshvardhan, D. A. Randall, T. G. Corsetti, and D. A. Dazlich, 1989: Earth radiation budget and cloudiness simulations with a general circulation model. *J. Atmos. Sci.,* **46,** 1922–1942.

Hartmann, D. L., H. H. Hendon, and R. A. Houze Jr., 1984: Some implications of the mesoscale circulations in tropical cloud clusters for large-scale dynamics and climate. *J. Atmos. Sci.,* **41,** 113–121.

Hendon, H. H., and M. L. Salby, 1994: The life cycle of the Madden–Julian oscillation. *J. Atmos. Sci.,* **51,** 2225–2237.

Houze, R. A., Jr., 1982: Cloud clusters and large-scale vertical motion in the tropics. *J. Meteor. Soc. Japan,* **60,** 396–410.

Johnson, R. H., 1980: Diagnosis of convective and mesoscale motions during Phase III of GATE. *J. Atmos. Sci.,* **37,** 733–753.

——, 1984: Partitioning tropical heat and moisture budgets into cumulus and meso-scale components: Implication for cumulus parameterization. *Mon. Wea. Rev.,* **112,** 1590–1601.

——, 1986: Short-term variations of the tropopause height over the winter MONEX area. *J. Atmos. Sci.,* **43,** 1152–1163.

——, and X. Lin, 1997: Episodic trade-wind regimes over the western Pacific warm pool. *J. Atmos. Sci.,* **54,** 2020–2034.

——, P. E. Ciesielski, and K. A. Hart, 1996: Tropical inversions near the 0°C level. *J. Atmos. Sci.,* **53,** 1838–1855.

Kalnay, E., and Coauthors, 1996: The NCEP/NCAR 40-Year Reanalysis Project. *Bull. Amer. Meteor. Soc.,* **77,** 437–471.

Lau, K.-M., P. J. Sheu, S. Schubert, D. Ledvina, and H. Weng, 1996: Evolution of large-scale circulation during TOGA COARE: Model intercomparison and basic features. *J. Climate,* **9,** 986–1003.

Lin, X., and R. H. Johnson, 1996a: Kinematic and thermodynamic characteristics of the flow over the western Pacific warm pool during TOGA COARE. *J. Atmos. Sci.,* **53,** 695–715.

——, and ——, 1996b: Heating, moistening and rainfall over the western Pacific warm pool during TOGA COARE. *J. Atmos. Sci.,* **53,** 3367–3383.

Lucas, C., and E. J. Zipser, 2000: Environmental variability during TOGA COARE. *J. Atmos. Sci.,* in press.

Lukas, R., P. J. Webster, M. Ji, and A. Leetma, 1995: The large-scale context for the TOGA Coupled Ocean–Atmosphere Response Experiment. *Meteor. Atmos. Phys.,* **56,** 3–16.

Madden, R. A., and P. R. Julian, 1971: Detection of a 40–50 day oscillation in the zonal wind in the tropical Pacific. *J. Atmos. Sci.,* **28,** 702–708.

Mapes, B. E., 1998: The large-scale part of tropical mesoscale convective system circulations: A linear vertical spectral band model. *J. Meteor. Soc. Japan,* **76,** 29–55.

McNab, A. L., and A. K. Betts, 1978: Mesoscale budget study of cumulus convection. *Mon. Wea. Rev.,* **106,** 1317–1331.

McPhaden, M. J., 1993: TOGA-TAO and the 1991–1993 ENSO event. *Oceanography,* **6,** 36–44.

Nakazawa, T., 1988: Tropical super clusters within intraseasonal variations over the west Pacific. *J. Meteor. Soc. Japan,* **66,** 777–786.

Nitta, T., 1972: Energy budget of wave disturbances over the Marshall Islands during the years of 1956 and 1958. *J. Meteor. Soc. Japan,* **50,** 71–84.

Nuss, W. A., and D. W. Titley, 1994: Use of multiquadric interpolation for meteorological objective analysis. *Mon. Wea. Rev.,* **122,** 1611–1631.

Ooyama, K. V., 1987: Scale-controlled objective analysis. *Mon. Wea. Rev.,* **115,** 2479–2506.

Parsons, D., and Coauthors, 1994: The Integrated Sounding System:

Description and preliminary observations from TOGA COARE. *Bull. Amer. Meteor. Soc.,* **75,** 553–567.
Pilewskie, P., and F. P. J. Valero, 1995: Direct observations of excess solar absorption by clouds. *Science,* **267,** 1626–1629.
Ramanathan, V., B. Subasilar, G. J. Zhang, W. Conant, R. D. Cess, J. T. Kiehl, H. Grassl, and L. Shi, 1995: Warm pool heat budget and shortwave cloud forcing: A missing physics? *Science,* **267,** 499–503.
Randall, D. A., Harshvardhan, D. A. Dazlich, and T. G. Corsetti, 1989: Interactions among radiation, convection, and large-scale dynamics in a general circulation model. *J. Atmos. Sci.,* **46,** 1943–1970.
Raymond, D. J., 2000: The Hadley circulation as a radiative-convective instability. *J. Atmos. Sci.,* **57,** 1286–1297.
Reed, R. J., 1978: The structure and behaviour of easterly waves over West Africa and the Atlantic. *Meteorology over the Tropical Oceans,* D. B. Shaw, Ed., Royal Meteorological Society, 57–71.
——, and E. E. Recker, 1971: Structure and properties of synoptic-scale wave disturbances in the equatorial western Pacific. *J. Atmos. Sci.,* **28,** 1117–1133.
Rossow, W. B., and R. A. Schiffer, 1991: ISCCP cloud data product. *Bull. Amer. Meteor. Soc.,* **72,** 2–20.
Sherwood, S. C., V. Ramanathan, T. P. Barnett, M. K. Tyree, and E. Roeckner, 1994: Response of an atmospheric general circulation model to radiative forcing of tropical clouds. *J. Geophys. Res.,* **99,** 20 829–20 845.
Sheu, R.-S., J. A. Curry, and G. Liu, 1996: Satellite retrieval of tropical rainfall using ISCCP analyses and microwave measurements. *J. Geophys. Res.,* **101,** 21 291–21 301.
Short, D. A., P. A. Kucera, B. S. Ferrier, J. C. Gerlach, S. A. Rutledge, and O. W. Thiele, 1997: Shipboard radar rainfall patterns within the TOGA COARE IFA. *Bull. Amer. Meteor. Soc.,* **78,** 2817–2836.
Slingo, A., and J. M. Slingo, 1988: The response of a general circulation model to cloud longwave radiative forcing. I: Introduction and initial experiments. *Quart. J. Roy. Meteor. Soc.,* **114,** 1027–1062.
——, and ——, 1991: The response of a general circulation model to cloud longwave radiative forcing. II: Further studies. *Quart. J. Roy. Meteor. Soc.,* **117,** 333–364.
Slingo, J. M., and R. A. Madden, 1991: Characteristics of the tropical intraseasonal oscillation in the NCAR community climate model. *Quart. J. Roy, Metoer. Soc.,* **117,** 1129–1169.
Stephens, G. L., 1996: How much solar radiation do clouds absorb? *Science,* **271,** 1131–1133.
——, A. Slingo, M. J. Webb, P. J. Minnett, P. H. Daum, L. Kleinman, I. Wittmeyer, and D. A. Randall, 1994: Observations of the Earth's radiation budget in relation to atmospheric hydrology. 4: Atmospheric column radiative cooling over the world's oceans. *J. Geophys. Res.,* **99,** 18 585–18 604.
Thompson, R. M., Jr., S. W. Payne, E. E. Recker, and R. J. Reed, 1979: Structure and properties of synoptic-scale wave disturbances in the intertropical convergence zone of the eastern Atlantic. *J. Atmos. Sci.,* **36,** 53–72.
Tiedtke, M., 1989: Comprehensive mass flux scheme for cumulus parameterization in large-scale models. *Mon. Wea. Rev.,* **117,** 1779–1800.
Trenberth, K. E., 1991: Climate diagnostics from global analyses: Conservation of mass in ECMWF analyses. *J. Climate,* **4,** 707–722.
——, J. W. Hurrell, and A. Solomon, 1995: Conservation of mass in three dimensions. *J. Climate,* **8,** 692–708.
Wade, C. G., and B. Schwartz, 1993: Radiosonde humidity observations near saturation. Preprints, *Eighth Symp. on Meteorological Observations and Instrumentation,* Anaheim, CA, Amer. Meteor. Soc., 44–49.
Webster, P. J., 1994: The role of hydrological processes in ocean–atmosphere interactions. *Rev. Geophys.,* **32,** 427–476.
——, and G. L. Stephens, 1980: Tropical upper-tropospheric extended clouds: Inferences from winter MONEX. *J. Atmos. Sci.,* **37,** 1521–1541.
——, and R. Lukas, 1992: TOGA COARE: The Coupled Ocean–Atmosphere Response Experiment. *Bull. Amer. Meteor. Soc.,* **73,** 1377–1416.
Weller, R. A., and S. P. Anderson, 1996: Surface meteorology and air–sea fluxes in the western equatorial Pacific during the TOGA Coupled Ocean–Atmosphere Response Experiment. *J. Climate,* **9,** 1959–1990.
Wong, T., G. L. Stephens, P. W. Stackhouse Jr., and F. P. J. Valero, 1993: The radiative budgets of a tropical mesoscale convective system during the EMEX-STEP-AMEX Experiment. 2: Model results. *J. Geophys. Res.,* **98,** 8695–8711.
Xie, P., and P. A. Arkin, 1997: Global precipitation: A 17-year monthly analysis based on gauge observations, satellite estimates, and numerical model outputs. *Bull. Amer. Meteor. Soc.,* **78,** 2539–2558.
Yanai, M., and R. H. Johnson, 1993: Impacts of cumulus convection on thermodynamic fields. *The Representation of Cumulus Convection in Numerical Models of the Atmosphere, Meteor. Monogr.,* No. 46, Amer. Meteor. Soc., 39–62.
——, S. Esbensen, and J. H. Chu, 1973: Determination of bulk properties of tropical cloud clusters from large-scale heat and moisture budgets. *J. Atmos. Sci.,* **30,** 611–627.
——, B. Chen, and W. Tung, 2000: The Madden–Julian oscillation observed during the TOGA COARE IOP: Global view. *J. Atmos. Sci.,* in press.
Yuter, S. E., and R. A. Houze Jr., 1995: Three-dimensional kinematic and microphysical evolution of Florida cumulonimbus. Part II: Frequency distributions of vertical velocity, reflectivity, and differential reflectivity. *Mon. Wea. Rev.,* **123,** 1941–1963.
Zipser, E. J., and R. H. Johnson, 1998: Systematic errors in radiosonde humidities: A global problem? Preprints, *10th Symp. on Meteorological Observations and Instrumentation,* Phoenix, AZ, Amer. Meteor. Soc., 72–73.